Journal of Power Sources 182 (2008) 359–364

Contents lists available at ScienceDirect

Journal of Power Sources

journal homepage: www.elsevier.com/locate/jpowsour

Short communication

Electrochemical deposition of porous Co_3O_4 nanostructured thin film for lithium-ion battery

Shu-Lei Chou[a,b,*], Jia-Zhao Wang[a,b], Hua-Kun Liu[a,b], Shi-Xue Dou[a]

[a] Institute for Superconducting and Electronic Materials, University of Wollongong, NSW 2522, Australia
[b] ARC Center of Excellence for Electromaterials Science, University of Wollongong, NSW 2522, Australia

ARTICLE INFO

Article history:
Received 3 December 2007
Accepted 25 March 2008
Available online 8 April 2008

Keywords:
Co_3O_4
Electrochemical deposition
Nanostructure
Porous
Thin film
Lithium-ion battery

ABSTRACT

Porous Co_3O_4 nanostructured thin films are electrodeposited by controlling the concentration of $Co(NO_3)_2$ aqueous solution on nickel sheets, and then sintered at 300 °C for 3 h. The as-prepared thin films are characterized by thermogravimetric analysis (TGA), X-ray diffraction (XRD), and scanning electron microscopy (SEM). The electrochemical measurements show that the highly porous Co_3O_4 thin film with the highest electrochemically active specific surface area (68.64 $m^2 g^{-1}$) yields the best electrochemical performance compared with another, less-porous film and with a non-porous film. The highest specific capacity (513 mAh g^{-1} after 50 cycles) is obtained from the thinnest film with Co_3O_4 loaded at rate of 0.05 mg cm^{-2}. The present research demonstrates that electrode morphology is one of the crucial factors that affect the electrochemical properties of electrodes.

1. Introduction

Rechargeable lithium-ion batteries are currently the technology of choice for portable electronic devices [1,2]. As one of the most important power supplies for micro-systems, thin-film lithium-ion batteries are of interest for important applications in a variety of consumer and medical products [3,4]. As one of the most promising anode materials [5–11] for such batteries, Co_3O_4, with a high theoretical capacity of 890 mAh g^{-1}, has been fabricated into thin films by various deposition methods, which include electrochemical deposition (ECD) [12,13], pulsed laser deposition (PLD) [14], sol–gel processing [15], electron beam evaporation [16], and radio frequency (RF) magnetron sputtering [17]. Among these methods, electrochemical deposition is a very convenient technique that forms nanostructured thin films with lower cost and higher performance at room temperature. Using electrochemical deposition, Liu and Yen [13] prepared Co_3O_4 thin-film electrodes for use in Li-ion batteries. These delivered an initial discharge capacity of 1930 mAh g^{-1} and a capacity of 500 mAh g^{-1} after 50 cycles. The reason for this high capacity is still not clear and has still to be confirmed. Furthermore, there has been no report on controlling the morphology of the Co_3O_4 thin film prepared by electrochemical deposition.

In this study, porous Co_3O_4 nanostructured thin films are prepared by controlling the parameters of electrochemical deposition on nickel sheets from $Co(NO_3)_2$ aqueous solution, that is then followed by sintering at 300 °C for 3 h. Electrochemical measurements show that the porous Co_3O_4 thin film formed from large nanoflakes gives the best performance, including high capacities and long cycle life, due to the high porosity and high electrochemically active surface area.

2. Experimental

Co_3O_4 thin films with different morphologies, namely, a porous film formed from large nanoflakes (Sample 1) (Fig. 1(a) and (b)), a porous film formed from small nanoflakes (Sample 2) (Fig. 1(c) and (d)), and a non-porous film with a smooth surface (Sample 3) (Fig. 1(e) and (f)), were prepared by galvanostatic electrochemical deposition at a current density of 1.0 mA cm^{-2} in 0.025, 0.1 and 0.0125 M $Co(NO_3)_2$, respectively, which was then followed by a heat-treatment at 300 °C for 3 h. Prior to electrodeposition, as working electrodes, nickel sheets were polished to a smooth surface, using successively finer grades of SiC paper, washed with distilled water, then ethanol, and finally dried in an air stream. Platinum foil was used as a counter electrode. The different concentrations of $Co(NO_3)_2$ solution were used as electrolytes. As precursors, $Co(OH)_2$ thin films were prepared by means of a gal-

* Corresponding author at: Institute for Superconducting and Electronic Materials, University of Wollongong, Northfields Avenue, Wollongong, NSW 2522, Australia. Tel.: +61 2 42215993; fax: +61 2 42215731.
E-mail address: sc478@uow.edu.au (S.-L. Chou).

0378-7753/$ – see front matter © 2008 Elsevier B.V. All rights reserved.
doi:10.1016/j.jpowsour.2008.03.083

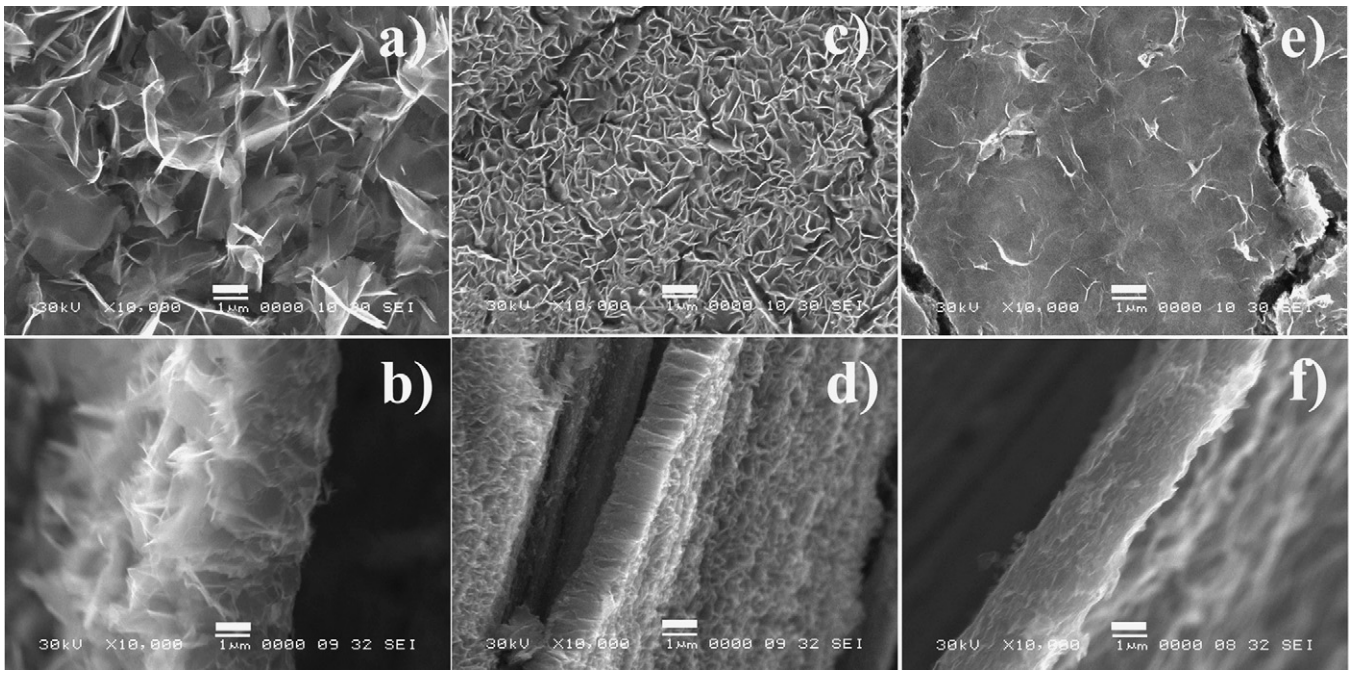

Fig. 1. SEM images of as-prepared Co_3O_4 thin films produced by electrochemical deposition at a current density of 1 mA cm^{-2} in 0.025 M (a and b), 0.1 M (c and d), and 0.0125 M (e and f) $Co(NO_3)_2$, followed by heat-treatment at 300 °C for 3 h. Scale bars are all 1 μm.

vanostatic technique at a current density of 1 mA cm^{-2} for 10 min. The possible reactions on the cathode electrode reported previously [18] are given in Eqs. (1)–(3). The porous $Co(OH)_2$ nanoflake thin films thus prepared were washed in de-ionized water three times, allowed to dry in air, and then heat-treated at 300 °C in air for 3 h:

$$NO_3^- + H_2O + 2e^- = NO_2^- + 2OH^- \quad (1)$$

$$NO_3^- + 7H_2O + 8e^- = NH_4^+ + 10OH^- \quad (2)$$

$$Co^{2+} + 2OH^- = Co(OH)_2 \quad (3)$$

The morphology and microstructure of the as-prepared Co_3O_4 thin films were characterized by X-ray diffraction (XRD) (GBC MMA 017), scanning electron microscopy (SEM) (JEOL JEM-3000), and thermogravimetric analysis (TGA) (TA 2000 Thermoanalyzer). Electrochemical measurements, which included charge–discharge test, cyclic voltammetry (CV) and electrochemical impedance spectroscopy (EIS), were obtained with a Neware battery test system and a CHI 660b electrochemistry workstation in conjunction with a three-electrode electrochemical cell. The electrochemical coin cell (CR 2032) contained samples on a Ni foil as the working electrode, a lithium foil as counter electrode and reference electrode, porous polypropylene as the separator, and 1 M $LiPF_6$ in a 50:50 (v/v) mixture of ethylene carbonate and dimethyl carbonate (MERCK KgaA, Germany) as the electrolyte. The cells were galvanostatically charged and discharged in the range of 0.01–2.0 V at constant current densities of 100, 200, and 400 mA g^{-1}.

3. Results and discussion

Fig. 1(a) shows an SEM image of Sample 1, which was formed from large nanoflakes of about 20–30 nm in thickness and several micrometers in length, whereas Fig. 1(b) shows a cross-sectional SEM image of Sample 1. It can be seen that Sample 1 has a total thickness of around 3 μm and a highly porous structure formed by nanoflakes which cross and connect with each other. Fig. 1(c) and (d) displays SEM images of Sample 2, which was formed from small nanoflakes of about 30–40 nm in thickness and less than 1 μm in length. The thickness of the Sample 2 film is only 1.5 μm, which indicates a much higher density and less porosity than Sample 1, due to the similar mass of Co_3O_4. SEM images of Sample 3 are presented in Fig. 1(e) and (f). From the former SEM, it can be seen that Sample 3 has the smoothest surface. The cross-sectional SEM image (Fig. 1(f)) shows that Sample 3 is of high density with a non-porous structure.

The thermostability of the product in air was studied by means of TGA analysis, shown in Fig. 2, and XRD patterns were used to characterize the intermediate products heated to different temperatures, as shown in Fig. 3(A) off and Fig. 3(B) on the substrate. The TGA results show a two-step weight-loss curve from 30 to 150 °C and from 150 to 400 °C. Both steps are characterized by XRD, as shown in Fig. 3(A). From 30 to 150 °C, the main weight-loss

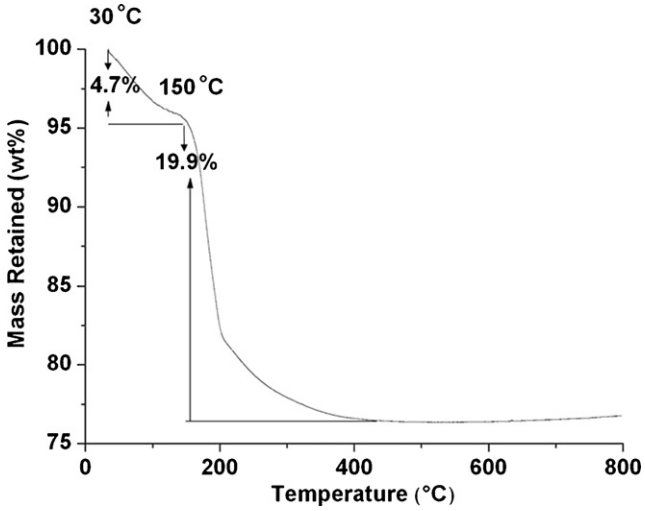

Fig. 2. TGA curve of as-obtained $Co(OH)_2$ films prepared by electrochemical deposition at heating rate of 5 °C min^{-1} from 30 to 800 °C in air.

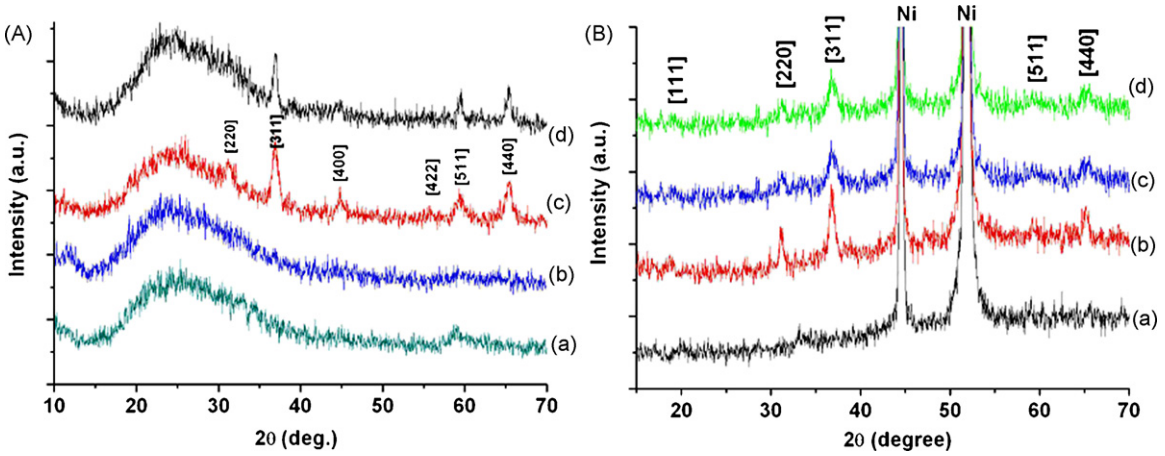

Fig. 3. XRD patterns of as-electrodeposited $Co(OH)_2$ films (A) off the substrate: air-dried (a) and sintered at 150 °C (b), 300 °C (c), and 400 °C (d) in air for 3 h, and (B) on the substrate: air-dried (a) and heat-treated at 300 °C for Sample 1 (b), Sample 2 (c), and Sample 3 (d).

arises from the evaporation of physically adsorbed water, and this is responsible for the similar XRD patterns (Fig. 3(A)) between the sample that was only air-dried and the one that was heat-treated at 150 °C, which indicates the same amorphous $Co(OH)_2$ structure. From 150 °C, $Co(OH)_2$ starts to transform into Co_3O_4. In the temperature range from 150 °C to approximately 400 °C, the weight-loss for the whole process is theoretically calculated to be 13.6% from Eq. (4), in comparison with the experimental value of 19.9%, due to the evaporation of water which might be inside the pores:

$$6Co(OH)_2 + 2O_2 = 2Co_3O_4 + 6H_2O \quad (4)$$

After sintering for 3 h at 300 °C, a satisfactory yield of polycrystalline Co_3O_4 is obtained and is indexed as a cubic phase of Co_3O_4 (ICDD-JCPDS card no.: 42-1467) with lattice constants $a = b = c = 8.0837$ Å, as evidenced from the XRD pattern shown in Fig. 3(A-c). The similar broad peaks from 20° to 35° originate from the glass substrate of the XRD sample holder. Fig. 2(B) shows the XRD patterns of Co_3O_4 thin films with different morphologies on the substrate after sintering for 3 h at 300 °C. There are only Co_3O_4 peaks, excluding the two peaks from the Ni substrate, which shows that the substrate is not oxidized after sintering. In addition, Sam-

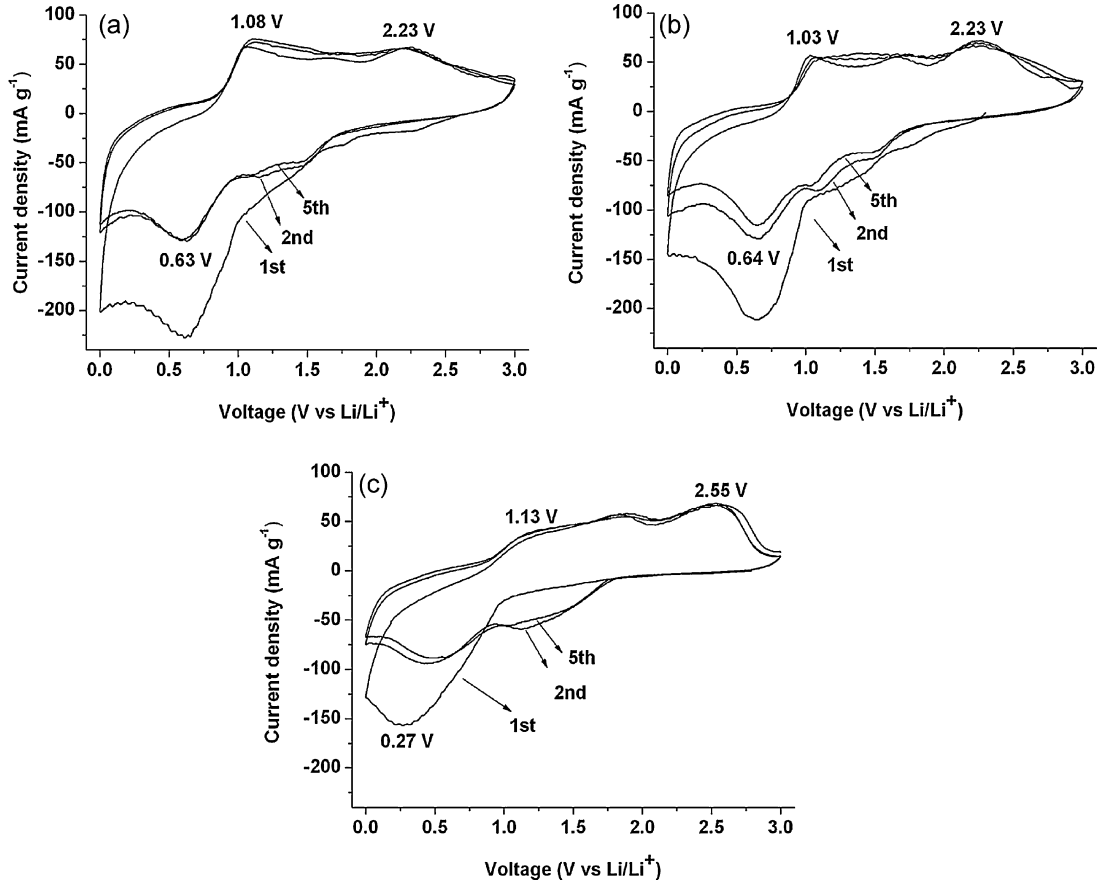

Fig. 4. Cyclic voltammograms of Sample 1 (a), Sample 2 (b) and Sample 3 (c) at scan rates of 0.1 mV s^{-1} for first, second and fifth cycles.

ple 1 exhibits the best crystal structure among the samples, despite the low intensity and weak crystallinity.

Fig. 4 displays cyclic voltammograms of Samples 1–3 at a scan rate of 0.1 mV s^{-1} between 0.0 and 3.0 V. The reactions between lithium and Co_3O_4 have been reported previously [7,8] and are expressed in Eqs. (5)–(7). In the first cycle, a maximum cathodic current peak at about 0.6 V and two main anodic peaks at 1.0 and 2.2 V reveal the different steps of the extraction process. The intensities of the cathodic peaks decrease in subsequent scanning cycles, due to the irreversible reaction (5) and the formation of a solid electrolyte interface (SEI) film. The intensities of the initial cathodic peak are in an order of $I_{Sample\,1} > I_{Sample\,2} > I_{Sample\,3}$, indicating that the initial discharge capacities should be in the same order. From the second to fifth cycle, the intensities of the cathodic peaks (around 0.6 V) of Sample 1 remain the same, showing the best cycle stability among the samples. One pair of quasi-reversible redox peaks is observed at around 0.6 and 1.05 V after the first cycle, so the charge–discharge range was chosen from 0.01 to 2.0 V for performance testing.

Initial discharge (lithiation):

$$Co_3O_4 + 8Li^+ + 8e^- \rightarrow 3Co + 4Li_2O \quad (5)$$

Charge (de-lithiation):

$$Co + Li_2O \rightarrow CoO + 2Li^+ + 2e^- \quad (6)$$

Discharge (lithiation):

$$CoO + 2Li^+ + 2e^- \rightarrow Co + Li_2O \quad (7)$$

Typical discharge–charge curves of the Co_3O_4 thin-film electrodes in Li-ion coin cells are shown in Fig. 5. The main reason for the existence of the initial irreversible capacity for anode materials is the formation of a solid electrolyte interface film, which forms on the surface of the anode material during the first discharge from 1.2 to 0.2 V [19,20]. As for Co_3O_4, the irreversible reaction (5) from Co_3O_4 to Co metal also contributes to the irreversible capacity [8,21]. The initial and second discharge capacities for Samples 1, 2 and 3 are 1129 and 812 mAh g^{-1}, 1090 and 770 mAh g^{-1}, and 1079 and 625 mAh g^{-1}, respectively. The retention of capacity for Samples 1, 2, and 3 is 71.9, 70.6, and 57.9%, respectively. Sample 1 shows the highest discharge capacities and highest retention of capacity, in good agreement with the CV tests.

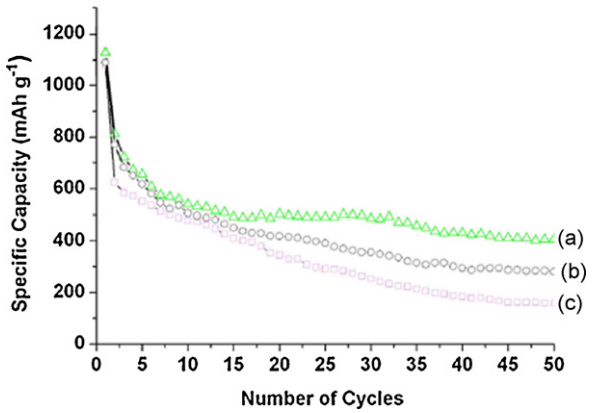

Fig. 6. Cycle life of Sample 1 (a), Sample 2 (b) and Sample 3 (c), at current density of 100 mA g^{-1}.

Fig. 6 presents the effect of cycling on the Co_3O_4 films at a current density of 100 mA g^{-1}. After 50 cycles, Sample 1 maintains 406 mAh g^{-1}, which corresponds to about 36% of initial discharge capacity and about 50% of second discharge capacity, while Samples

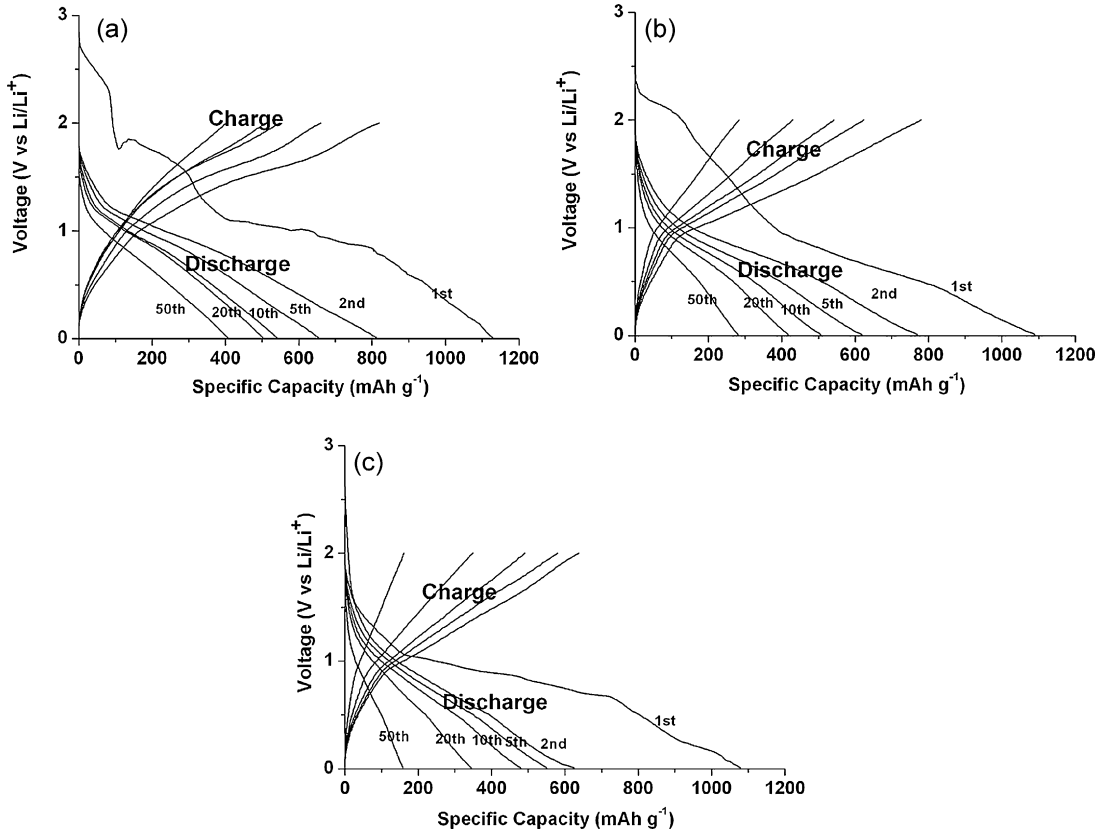

Fig. 5. Typical charge–discharge curves of Sample 1 (a), Sample 2 (b) and Sample 3 (c).

Table 1
Specific capacities of large nanoflake porous Co_3O_4 films (Sample 1) with different masses of Co_3O_4 obtained by controlling the time of electrochemical deposition with different charge–discharge rates

Mass of Co_3O_4 (mg cm^{-2})	Current density (mA g^{-1})	Specific capacity (mAh g^{-1})				
		Initial	2nd	10th	20th	50th
0.05	100	1430	863	605	568	513
0.15	100	1291	840	577	542	453
0.31	100	1129	811	540	502	406
0.31	200	931	722	503	465	351
0.31	400	826	664	445	421	318

2 and 3 only yield 218 and 158 mAh g^{-1}, respectively. The capacity loss (CL) is in the order of $CL_{Sample\,1} < CL_{Sample\,2} < CL_{Sample\,3}$. Thus, the morphologies affect not only the discharge capacity, but also the cycleability of Li-ion batteries. Porous and nanostructured films show the highest capacity and the best cycle life.

By controlling the time of electrochemical deposition (while the other conditions were the same as for Sample 1), porous Co_3O_4 nanoflake thin films with different masses of Co_3O_4 were prepared; the specific capacities of the different masses of Co_3O_4 and different charge–discharge rates are summarized in Table 1. It can be seen that the thinnest film shows the highest specific capacity and the best cycle life. After 50 cycles, the thin film with a Co_3O_4 mass of 0.05 mg cm^{-2} delivers a specific capacity of 513 mAh g^{-1}, which is similar to the result reported by Liu and Yen [13]. At a higher current density (400 mA g^{-1}) for both charge and discharge, the porous Co_3O_4 nanoflake thin film still yields a higher initial specific capacity of 826 mAh g^{-1} and also a relatively higher capacity of 318 mAh g^{-1} after 50 cycles. These findings demonstrate a significantly higher rate of charge–discharge performance.

The electrochemically active specific surface area (S_E, m^2 g^{-1}) can be calculated from the specific capacitance of the electrochemical double layer (C_{dm}, F g^{-1}), by means of the relationship $S_E = C_{dm}/C_d$, where C_d is the capacitance of the electrochemical double layer, with a constant value of 20 μF cm^{-2}. The value of C_{dm} can be obtained from electrochemical impedance spectra at low frequency (0.01 Hz) in accordance with the equation $C_{dm} = (2\pi f m Z_{Img})^{-1}$, where f (Hz) is the frequency, m (g) is the mass of the active materials, and Z_{Img} (Ω) is the imaginary part of the impedance. The EIS were obtained over a frequency range from 1 MHz to 0.01 Hz at 3.2 V (vs. Li/Li$^+$), because there is no electrochemical reaction between lithium and Co_3O_4 above 3.0 V [13,14]. The Bode plots from the impedance spectra of Samples 1, 2 and 3 are shown in Fig. 7, indicating the relationship between C_{dm} and f. From the spectra, it can be seen that the value of C_{dm} for Sample 1 is 13.7 F g^{-1}, which is the highest among the samples. The calculated values of S_E for Samples 1, 2 and 3 are listed in Table 2. Sample 1 exhibits the highest electrochemically active specific surface area

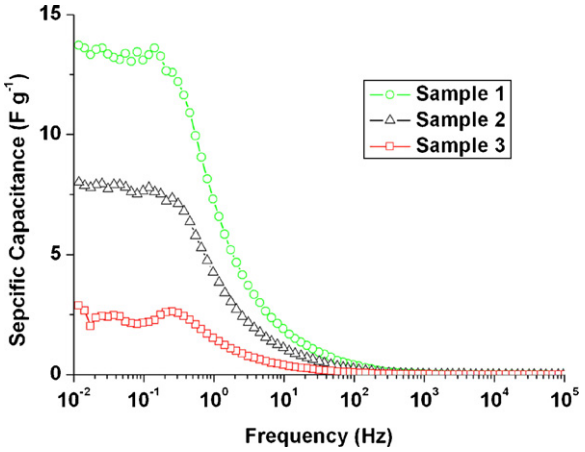

Fig. 7. Bode plots from impedance spectra of Samples 1, 2 and 3 at 3.2 V (vs. Li/Li$^+$).

Table 2
Electrochemically active specific surface area (S_E) calculated from EIS

	f(Hz)	C_{dm} (F g^{-1})	S_E (m^2 g^{-1})
Sample 1	0.01	13.73	68.64
Sample 2	0.01	8.00	40.01
Sample 3	0.01	2.87	14.37

(68.6 m^2 g^{-1}), which is consistent with SEM observations. That is, the large nanoflakes form the most porous Co_3O_4 films (Sample 1) which have the highest electrochemically active specific surface area. This is also the reason why Sample 1 shows the best electrochemical performance, including the highest capacity and the best cycle life.

After 50 charge–discharge cycles, the Co_3O_4 thin films were taken out of the coin cell. Fig. 8 gives the SEM images after cycling for (a) Sample 1, (b) Sample 2 and (c) Sample 3. Compared with the SEM images shown in Fig. 1, which were taken before cycling, the morphologies of three samples have all changed. For Sample 1, although some of the large nanoflakes have collapsed, there are still some smaller nanoflakes which can maintain the porous structure. Sample 1 exhibits the best cycle life due to benefitting from the preservation of the porous structure. For Sample 2, the pores became small, and some pores were even blocked. This is why the capacities keep falling. For Sample 3, it appears that the electrochemical reaction occurs only on the surface of the electrode, because there are some small and thin nanoflakes formed on the surface of electrode compared with the smooth surface shown in Fig. 1(e). The electrolyte is not able to penetrate the deeper materials, so the capacity will naturally be the lowest one.

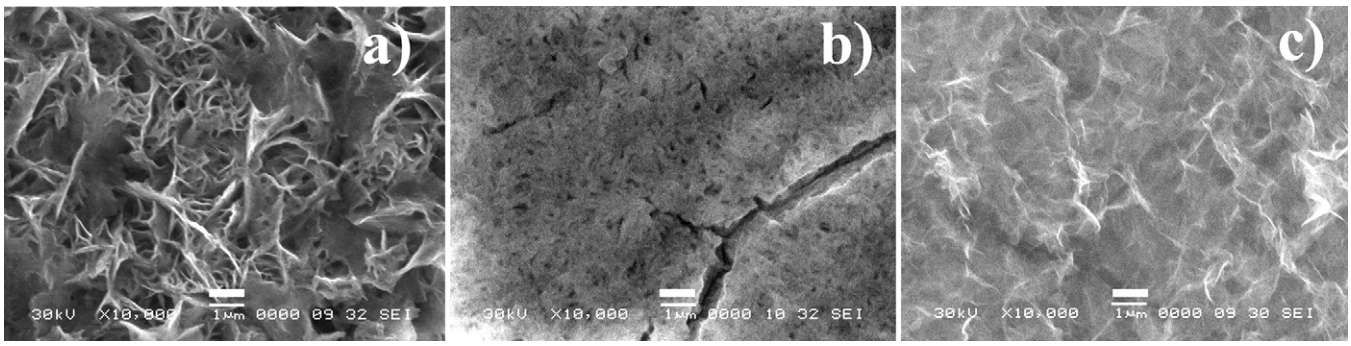

Fig. 8. SEM images of Co_3O_4 thin films after charge–discharge over 50 cycles for (a) Sample 1, (b) Sample 2 and (c) Sample 3. Scale bars are all 1 μm.

4. Conclusions

Porous Co_3O_4 nanostructured thin films are electrodeposited by controlling the concentration of $Co(NO_3)_2$ aqueous solution on nickel sheets, and then sintered at 300 °C for 3 h. The electrochemical measurements show that the porous Co_3O_4 thin film formed from large nanoflakes has the highest electrochemically active specific surface area ($68.64\,m^2\,g^{-1}$) and shows the best electrochemical performance, including the highest capacity and longest cycle life, due to the porous nanostructure, compared with the other two films, one less porous and the other non-porous. The pores and nanostructures of Sample 1 show little change after 50 cycles. The highest specific capacity of $513\,mAh\,g^{-1}$ after 50 cycles is obtained from the thinnest film, with Co_3O_4 loaded at the rate of $0.05\,mg\,cm^{-2}$. This method could also be used to improve the electrochemical properties of other metal oxides for lithium-ion batteries.

Acknowledgments

Financial support provided by the Australian Research Council (ARC) through ARC Centre of Excellence funding (CE0561616) is gratefully acknowledged. The authors thank Dr. T. Silver at the University of Wollongong for critical reading of the manuscript.

References

[1] J.M. Tarascon, M. Armand, Nature 414 (2001) 359–367.
[2] M. Winter, R.J. Brodd, Chem. Rev. 104 (2004) 4245–4269.
[3] (a) J.B. Bates, G.R. Gruzalski, N.J. Dudney, C.F. Luck, X.H. Yu, Solid State Ionics 70–71 (1994) 619–628;
(b) J.B. Bates, N.J. Dudney, B. Neudecker, A. Ueda, C.D. Evans, Solid State Ionics 135 (2000) 33–45.
[4] G.J. La O', H.J. In, E. Crumlin, G. Barbastathis, Y. Shao-Horn, Int. J. Energy Res. 31 (2007) 548–575.
[5] P. Poizot, S. Laruelle, S. Grugeon, L. Dupont, J.-M. Tarascon, Nature 407 (2000) 496–499.
[6] F. Badway, I. Plitz, S. Grugeon, S. Laruelle, M. Dolle', A.S. Gozdz, J.M. Tarascon, Electrochem. Solid State Lett. 5 (2002) A115–A118.
[7] G.X. Wang, Y. Chen, K. Konstantinov, M. Lindsay, H.K. Liu, S.X. Dou, J. Power Sources 109 (2002) 142–147.
[8] D. Larcher, G. Sudant, J.-B. Leriche, Y. Chabre, J.-M. Tarascon, J. Electrochem. Soc. 149 (2002) A234–A241.
[9] W.Y. Li, L.N. Xu, J. Chen, Adv. Funct. Mater. 15 (2005) 851–857.
[10] K.T. Nam, D.W. Kim, P.J. Yoo, C.Y. Chiang, N. Meethong, P.T. Hammond, Y.M. Chiang, A.M. Belcher, Science 312 (2006) 885–888.
[11] G. Binotto, D. Larcher, A.S. Prakash, R.H. Urbina, M.S. Hegde, J.M. Tarascon, Chem. Mater. 19 (2007) 3032–3040.
[12] C.N. Polo da Fonseca, M.A. de Paoli, A. Gorenstein, Adv. Mater. 3 (1991) 553–555.
[13] H.C. Liu, S.K. Yen, J. Power Sources 166 (2007) 478–484.
[14] (a) Y. Wang, Z.-W. Fu, Q.-Z. Qin, Thin Solid Films 441 (2003) 19–24;
(b) Z.W. Fu, Y. Wang, Y. Zhang, Q.Z. Qin, Solid State Ionics 170 (2004) 105–109.
[15] F. Svegl, B. Orel, I.G. Svegl, V. Kaucic, Electrochim. Acta 45 (2000) 4359–4371.
[16] T. Seike, J. Nagai, Solar Energy Mater. 22 (1991) 107–117.
[17] C.L. Liao, Y.H. Lee, S.T. Chang, K.Z. Fung, J. Power Sources 158 (2006) 1379–1385.
[18] G.H.A. Therese, P.V. Kamath, Chem. Mater. 12 (2000) 1195–1204.
[19] F. Orsini, A. Du Pasquier, B. Beaudoin, J.M. Tarascon, M. Trentin, N. Langenhuizen, E. De Beer, P. Notten, J. Power Sources 76 (1998) 19–29.
[20] H. Li, L.H. Shi, Q. Wang, L.Q. Chen, X.J. Huang, Solid State Ionics 148 (2002) 247–258.
[21] (a) Y.M. Kang, K.T. Kim, K.Y. Lee, S.J. Lee, J.H. Jung, J.Y. Lee, J. Electrochem. Soc. 150 (2003) A1538–A1543;
(b) Y.M. Kang, K.T. Kim, J.H. Kim, H.S. Kim, P.S. Lee, J.Y. Lee, H.K. Liu, S.X. Dou, J. Power Sources 133 (2004) 252–259.